Novel Families of Three-Component Reversible Redox Cycles Involving Cage Deformation via Intramolecular Redox Reaction: Tetrathiolate-Bridged Dinuclear Molybda- and Tungstacarboranes[†]

Jeong-Wook Hwang, Jae-Hak Kim, Hangil Lee, Hochun Lee, Sehun Kim,* Juhyoun Kwak,* and Youngkyu Do*

Contribution from the Department of Chemistry, School of Molecular Science-BK21 and Center for Molecular Design and Synthesis, Korea Advanced Institute of Science and Technology, Daejeon 305-701, Korea

Received March 8, 2001

Abstract: The synthesis and structural analysis of two novel families of three-component reversible redox cycles $[(C_2B_9H_{11})M(\mu\text{-SPh})_2]_2{}^n PPN_n$ (M = Mo, $n = 2-$, **2**; $1-$, **3**; 0, **4**; and M = W, $n = 2-$, **6**; $1-$, **7**; 0, **8**), where the cleavage and re-formation of the carborane cage C–C bond is observed during the redox reaction, are reported. Electronic saturation of the metal center (18e center) and the lack of bulky substituents on the carborane cage suggest that the deformed carborane cages in **2**·PPN₂, **6**·PPN₂, and **7**·PPN invoke a new kind of deformed cage ("semicloso" framework). The XPS results show that the unprecedented competition for electron density between the metal center and the carborane cage is involved in the cleavage and formation of the carborane C–C bond.

Introduction

Since the first report of the metallacarborane $[(C_2B_9H_{11})_2Fe]^{2-}$ by Hawthorne et al.,[1] the chemistry of metallacarboranes has expanded in both scope and diversity and has provided a rich field of study and applications.[2] Probably the most exciting feature of metallacarborane clusters is their extremely rich structural variance that has not been observed in other ligand systems. One of the most interesting and unusual structural features in some metallacarborane systems is the cleavage of the cage C–C bond.[3] The first synthesis and structural characterization of the cage C–C cleaved metallacarborane [Fe₂-Cp₂(C₂B₆H₈)][4] led to a number of the dicarbollide compounds which show the cage C–C bond cleavage.[5–8]

The compounds with the cage C–C bond cleavage can be classified into two classes, hypercloso (alternatively, isocloso) and pseudocloso, according to the type of the driving force for the C–C cleavage: The hypercloso system derives its driving force from the electronic effect (unsaturation of the metal center),[5] while the pseudocloso system is driven by the steric effects.[8] The metallacarborane clusters in these systems are related to the closo species by the proposed diamond–square–diamond (DSD) process.[9] In addition to the electronically driven C–C bond cleavage of the dicarbollide cage, the parent C_2B_{10} cage is also known to undergo reduction, suffering severe distortion as well as leading to new ligand systems.[10,11] On the other hand, the dicarbollide ligand can also act as an electron buffer and thus shows supreme stabilizing power for both low and high oxidation state metals.[2] These two features, cage distortion vs electron buffer, of the dicarbollide ligand raise the necessity of probing the electron flow between the cage and the metal that occurs during cage distortion. For this purpose, we have focused our research interest on the structural change of the Group 6 metallacarborane clusters during redox reaction, leading to the observation of systems where the competition for electron between the dicarbollide cage and the metal center is involved during the redox reactions. Herein, we report the details of the syntheses, structures, and intramolecular redox properties probed by the X-ray photoelectron spectra (XPS) of two novel families of three-component reversible redox cycles $[(C_2B_9H_{11})M(\mu\text{-SPh})_2]_2{}^n$ (M = Mo, W; $n = 2-$, $1-$, 0). Preliminary reports on the synthesis and structures for M = Mo with $n = 2-$ and $1-$ have been communicated.[12] The observed metallacarboranes provide the first examples of the cage C–C bond cleavage in the nonsubstituted 12-vertex

[†] For the purpose of clear structural comparison, the same atom numbering scheme was used for all complexes in this paper.

(1) Young, D. C.; Wegner, P. A.; Hawthorne, M. F. *J. Am. Chem. Soc.* **1965**, *87*, 1818.

(2) For recent reviews, see: (a) Saxena, A. K.; Maguire, J. A.; Hosmane, N. S. *Chem. Rev.* **1997**, *97*, 2421. (b) Plešek, J. *Chem. Rev.* **1992**, *92*, 269. (c) Saxena, A. K.; Hosmane, N. S. *Chem. Rev.* **1993**, *93*, 1081. (d) Grimes, R. N. In *Comprehensive Organometallic Chemistry II*; Abel, E. W., Stone, F. G. A., Wilkinson, G., Eds; Pergamon: Oxford, U.K., 1995; Vol. 1, p 371. (e) Grimes, R. N. *Coord. Chem. Rev.* **2000**, *200–202*, 773.

(3) Similar distortion is also observed in the metallaborane cluster. One (in the case of 11- and 10-vertex clusters) or two (in the case of a 9-vertex cluster) of the cluster B–B bonds are cleaved, resulting in a six-membered open face.

(4) Callahan, K. P.; Evans, W. J.; Lo, F. Y.; Strouse, C. E.; Hawthorne, M. F. *J. Am. Chem. Soc.* **1975**, *97*, 296.

(5) (a) Jung, C. W.; Baker, R. T.; Knobler, C. B.; Hawthorne, M. F. *J. Am. Chem. Soc.* **1980**, *102*, 5782. (b) Jung, C. W.; Baker, R. T.; Hawthorne, M. F. *J. Am. Chem. Soc.* **1981**, *103*, 810.

(6) Attfield, M. J.; Howard, J. A. K.; Jelfs, A. N. de M.; Nunn, C. M.; Stone, F. G. A. *J. Chem. Soc., Dalton Trans.* **1987**, 2219.

(7) Carr, N.; Mullica, D. F.; Sappenfield, E. L.; Stone, F. G. A. *Organometallics* **1992**, *11*, 3697.

(8) See: Thomas, R. L.; Welch, A. J. *J. Chem. Soc., Dalton Trans.* **1997**, 631 and references therein.

(9) Lipscomb, W. N. *Science* **1966**, *153*, 373.

(10) Dustin, D. F.; Dunks, G. B.; Hawthorne, M. F. *J. Am. Chem. Soc.* **1973**, *95*, 1109.

(11) Xie, Z.; Yan, C.; Yang, Q.; Mak, T. C. W. *Angew. Chem., Int. Ed.* **1999**, *38*, 1761.

(12) Kim, J.-H.; Lamrani, M.; Hwang, J.-W.; Do, Y. *Chem. Commun.* **1997**, 1761.

Three-Component Reversible Redox Cycles

J. Am. Chem. Soc., Vol. 123, No. 37, 2001 9055

systems which invoke the presence of a new kind of deformed cage ("semicloso" framework), driven by the intramolecular redox reaction.

Experimental Section

General Procedures and Materials. All manipulations were carried out under dinitrogen by using standard Schlenk techniques. Reagent grade solvents were distilled from appropriate drying agents,[13] and deuterated DMSO was dried from activated molecular sieve 3A. Mo-$(CO)_6$, $W(CO)_6$, phenyl disulfide, n-Bu_4NPF_6, bis(triphenylphospho-ranylidene)ammonium chloride (PPNCl), silver acetate, CuCl, and potassium were purchased from Aldrich and used as received. $FeCl_3$ was purchased from Cerac and was dissolved in MeOH and filtered before use to remove the insoluble dark precipitates. The surface of potassium was cleaned before use by refluxing in THF.

Synthesis. $[(C_2B_9H_{11})Mo(\mu$-$SPh)_2]_2PPN_2$ ($2\cdot PPN_2$). Excess PhSSPh (260 mg, 1.2 mmol) was added to an in situ generated orange solution of $[(C_2B_9H_{11})Mo(CO)_3]\cdot PPN_2$ ($1\cdot PPN_2$) (700 mg, 0.50 mmol)[14] in 40 mL of MeCN. The reaction mixture was refluxed for 24 h, and the gradual formation of yellow crystalline precipitate was observed. All solvent was removed by vacuum, and the residue was washed with 30 mL of THF (3 times) and 20 mL of MeOH (3 times). The yellow residue was recrystallized from DMF/Et$_2$O, affording analytically pure orange yellow crystals of $2\cdot PPN_2$ in a yield of 41% (200 mg). Crystals suitable for X-ray crystallography were obtained by layer diffusion of Et$_2$O to the DMF solution of $2\cdot PPN_2$. Anal. Calcd for $C_{100}H_{102}N_2B_{18}P_4S_4$-$Mo_2$: C, 60.95; H, 5.22; N, 1.42. Found: C, 60.50; H, 5.28; N, 1.37. IR (KBr, cm^{-1}): ν_{BH} = 2526, 2498, 2470, and 2449. ^{1}H NMR (ppm, DMSO-d_6): 3.63 (br, 1H, carboranyl CH), 3.92 (br, 1H, carboranyl CH), 6.9−7.3 (m, 10H, phenyl of C_6H_5S), and 7.5−7.7 (m, 30H, phenyl of PPN). ^{11}B{^{1}H} NMR (ppm, DMSO-d_6, 110 °C): 1.38, −3.12, −7.11, and −20.55 (3:4:1:1). Electronic spectrum (DMF): 402 nm (ϵ 13 000).

$[(C_2B_9H_{11})Mo(\mu$-$SPh)_2]_2PPN$ ($3\cdot PPN$). An excess amount of CuCl (210 mg, 2.1 mmol) was added to a yellow slurry of $2\cdot PPN_2$ (1.7 g, 0.86 mmol) in 70 mL of CH_2Cl_2. The color of the reaction mixture gradually turned black. After the mixture was stirred for 10 h, the gray metallic precipitates were filtered off using a Celite bed, and the black filtrate was concentrated to dryness. The black residue was washed with 20 mL of MeOH (2 times) and 15 mL of Et$_2$O (2 times), and the recrystallization in DMF/MeOH gave analytically pure black single crystals of $3\cdot PPN$ in a yield of 86% (1.1 g). Anal. Calcd for $C_{64}H_{72}$-$NB_{18}P_2S_4Mo_2$: C, 53.68; H, 5.07; N, 0.98. Found: C, 53.42; H, 5.15; N, 0.85. IR (KBr, cm^{-1}): ν_{BH} = 2580 (sh), 2552, and 2522. Electronic spectrum (DMF): 946 (ϵ 110), 686 (ϵ 430), 577 (ϵ 1300), and 395 nm (ϵ 8200) (sh).

$[(C_2B_9H_{11})Mo(\mu$-$SPh)_2]_2$ (4). (A) Reaction of $3\cdot PPN$ with Excess $FeCl_3$. To a black solution of $3\cdot PPN$ (290 mg, 0.20 mmol) in 80 mL of CH_2Cl_2 was added a solution of excess $FeCl_3$ (50 mg, 0.31 mmol) in 20 mL of MeOH. Green microcrystals formed immediately. The reaction mixture was stirred for 4 h and filtered. Green microcrystalline residue (130 mg, 0.14 mmol, yield 72%) was washed with 30 mL of MeOH (3 times), 10 mL of CH_2Cl_2 (3 times), and 10 mL of Et$_2$O (2 times) and dried by blowing N_2 over it. Crystals suitable for X-ray study were obtained by layer diffusion of a solution of $FeCl_3$ in MeOH to a solution of $3\cdot PPN$ in CH_2Cl_2. Anal. Calcd for $C_{28}H_{42}B_{18}S_4Mo_2$: C, 37.64; H, 4.74. Found: C, 37.80; H, 4.87. IR (KBr, cm^{-1}): ν_{BH} = 2633, 2587, 2574, 2558, 2544, 2530, and 2517. Electronic spectrum (THF): 1105 (ϵ 5700), 630 (ϵ 2100), and 450 nm (sh).

(B) Reaction of $2\cdot PPN_2$ with Excess $FeCl_3$. To a yellow slurry of $2\cdot PPN_2$ (200 mg, 0.10 mmol) in 30 mL of CH_2Cl_2 was added a solution of an excess amount of $FeCl_3$ (150 mg, 0.93 mmol) in 30 mL of MeOH. Immediate formation of green microcrystals was observed. The reaction mixture was stirred for 4 h and filtered. Green microcrystalline product **4** (65 mg, 0.073 mmol, yield 72%) was washed with 30 mL of MeOH (3 times), 10 mL of CH_2Cl_2 (3 times), and 10 mL of Et$_2$O (2 times)

and dried by blowing N_2 over it. All spectroscopic data are the same as those from the oxidation of $3\cdot PPN$ with excess $FeCl_3$.

Reduction of $3\cdot PPN$. To a slurry of $3\cdot PPN$ (110 mg, 0.073 mmol) in 50 mL of THF was added an excess amount (26 mg, 0.67 mmol) of potassium. The reaction mixture was refluxed for 3 h, resulting in a yellow solution with yellow microcrystals. The residual potassium was removed mechanically, and an excess amount (300 mg, 0.52 mmol) of PPNCl was added. The reaction mixture was stirred for 12 h, and 2-propanol was added slowly to remove any remaining potassium until the evolution of gas was not observed. After decanting of the solution, the resulting orange-yellow precipitate was washed with 10 mL of MeOH (3 times) and extracted by 10 mL of DMF. Pouring 50 mL of Et$_2$O into the DMF solution gave yellow microcrystals (90 mg) of $2\cdot$ PPN_2 in a yield of 62%.

Reduction of 4. (A) Reaction of 4 with Potassium. An excess amount of potassium (36 mg, 0.92 mmol) was added to a slurry of **4** (58 mg, 0.065 mmol) in 50 mL of THF. Reflux of the solution caused the color to change to black in 2 h and then to yellow. After 12 h of refluxing, the residual potassium was removed mechanically, and excess PPNCl (500 mg, 0.86 mmol) was added. After 4 h of stirring, 2-propanol was added slowly to the reaction mixture to remove residual potassium. After filtering, the residual yellow precipitate was collected, washed with 10 mL of MeOH (3 times), and extracted with 15 mL of DMF. Precipitation by pouring 50 mL of Et$_2$O gave yellow microc-rystals of $2\cdot PPN_2$ in a yield of 55% (70 mg, 0.036 mmol).

(B) Reaction of 4 with $2\cdot PPN_2$. $2\cdot PPN_2$ (160 mg, 0.080 mmol) and **4** (72 mg, 0.081 mmol) were stirred in a mixed solvent of THF and CH_2Cl_2 (1:2). The mixture gradually turned black, and after 2 h of stirring, all solvent was evaporated and the resulting black residue was extracted by 20 mL of CH_2Cl_2. Pouring 60 mL of Et$_2$O into the mixture gave black microcrystals of $3\cdot PPN$. The black microcrystals (180 mg, 0.13 mmol, yield 79%) were washed with 10 mL of MeOH and 20 mL of Et$_2$O.

Reaction of $2\cdot PPN_2$ with PMe$_3$. A 1.4 mL portion of a 1 M toluene solution of PMe$_3$ (1.4 mmol, 10 equiv with respect to Mo atom) was added to $2\cdot PPN_2$ (144 mg, 0.0731 mmol) dissolved in 30 mL of DMF. The reaction mixture was heated to 85 °C for one week. No change in color or formation of precipitates was observed during that period. The reaction mixture was filtered, and the concentrated filtrate was treated with 100 mL of Et$_2$O to give 132 mg (0.0670 mmol) of yellow microcrystalline powder. The spectroscopic data of the yellow powder were the same as those of $2\cdot PPN_2$, showing that the starting compound $2\cdot PPN_2$ was recovered in 92% yield.

Reaction of $2\cdot PPN_2$ with CNBu^t. To a DMF solution (20 mL) of $2\cdot PPN_2$ (180 mg, 0.090 mmol) was added 10 equiv of CNBu^t (0.21 mL, 2.0 mmol) with respect to Mo atoms. After the reaction mixture was stirred at 85 °C for one week, it was filtered. The filtrate was concentrated to 10 mL and treated with 100 mL of Et$_2$O. The resulting yellow crystalline powder (160 mg, 0.082 mmol, $2\cdot PPN_2$ recovered in 91% yield) showed spectroscopic data identical with those of the starting material.

$[(C_2B_9H_{11})W(\mu$-$SPh)_2]_2PPN_2$ ($6\cdot PPN_2$). An excess amount (2.3 g, 10 mmol) of PhSSPh was added to an in situ generated orange MeCN solution of $[(C_2B_9H_{11})W(CO)_3]\cdot PPN_2$ ($5\cdot PPN_2$) (4.4 g, 3.0 mmol).[15] The reaction mixture was refluxed for 72 h, and gradual formation of a yellow crystalline precipitate was observed. All solvent was removed in vacuo, and the residue was washed with 30 mL of THF (3 times) and 20 mL of MeOH (3 times). The yellow residue was recrystallized from DMF/Et$_2$O, affording analytically pure orange-yellow crystals of $6\cdot PPN_2$ in a yield of 32% (1.03 g, 0.480 mmol). Crystals suitable for X-ray crystallography were obtained by layer diffusion of Et$_2$O to a DMF solution of $6\cdot PPN_2$. Anal. Calcd for $C_{100}H_{102}N_2B_{18}P_4S_4W_2$: C, 55.96; H, 4.79; N, 1.31. Found: C, 55.97; H, 4.97; N, 1.37. IR (KBr, cm^{-1}): ν_{BH} = 2526, 2497, 2468, and 2445. ^{1}H NMR (ppm, DMSO-d_6): 4.58 (br, 1H, carboranyl CH), 4.17 (br, 1H, carboranyl CH), 6.9−7.3 (m, 10H, phenyl of C_6H_5S), and 7.5−7.7 (m, 30H, phenyl of PPN). ^{11}B{^{1}H} NMR (ppm, DMSO-d_6, 110 °C): 15.02, 8.88, −1.88, −5.85, −9.65, and −20.18 (1:1:2:2:2:1). Electronic spectrum (DMF): 382 nm (ϵ 19 000).

(13) Perrin, D. D.; Armarego, W. L. F.; Ferrin, D. R. *Purification of Laboratory Chemicals*, 2nd ed.; Pergamon: New York, 1980.

(14) Kim, J.-H.; Lamrani, M.; Hwang, J.-W.; Do, Y. *Inorg. Chim. Acta* **1998**, *283*, 145.

(15) $5\cdot PPN_2$ was generated in analogy to the generation of $1\cdot PPN_2$.

9056 *J. Am. Chem. Soc., Vol. 123, No. 37, 2001*

Hwang et al.

[(C₂B₉H₁₁)W(μ-SPh)₂]₂PPN (7·PPN). An excess amount of silver acetate (0.30 g, 1.9 mmol) was added to a yellow slurry of **6·PPN₂** (0.60 g, 0.28 mmol) in 70 mL of CH₂Cl₂. The color of the reaction mixture gradually turned to dark brown. After being stirred for 10 h, the reaction mixture was concentrated to dryness and washed with 30 mL of MeOH (3 times). The resulting dark brown solid was dissolved in 50 mL of CH₂Cl₂ and filtered twice through the PTFE membrane filter (0.45 μm). The dark brown solution was concentrated to ca. 30 mL and treated with 100 mL of MeOH. The resulting dark brown crystals were collected and washed with 20 mL of MeOH (2 times) and 15 mL of Et₂O (2 times) to give the analytically pure dark brown crystals (which were suitable for X-ray study) of **7·PPN** in a yield of 86% (390 mg, 0.24 mmol). Anal. Calcd for C₆₄H₇₂NB₁₈P₂S₄W₂: C, 48.18; H, 4.55; N, 0.96. Found: C, 47.81; H, 4.51; N, 0.87. IR (KBr, cm⁻¹): ν_{BH} = 2594 (sh), 2574 (sh), 2560, 2517, and 2480. Electronic spectrum (DMF): 795 (ε 260), 602 (ε 810), 510 (ε 1800), and 358 nm (ε 13 000).

[(C₂B₉H₁₁)W(μ-SPh)₂]₂ (8). (A) Reaction of 7·PPN with Excess FeCl₃. To a dark brown solution of **7·PPN** (81 mg, 0.050 mmol) in 50 mL of CH₂Cl₂ was added excess FeCl₃ (120 mg, 0.74 mmol) in 20 mL of MeOH. Red-purple microcrystals formed immediately. The reaction mixture was stirred for 4 h and filtered. The red-purple microcrystalline residue (39 mg, 0.036 mmol, yield 72%) was washed with 30 mL of MeOH (3 times), 10 mL of CH₂Cl₂ (3 times), and 10 mL of Et₂O (2 times) and dried by blowing N₂ over it. Crystals suitable for X-ray crystallography were obtained by layer diffusion of FeCl₃ in MeOH to **7·PPN** in CH₂Cl₂. Anal. Calcd for C₂₈H₄₂B₁₈ S₄W₂: C, 31.45; H, 3.96. Found: C, 31.66; H, 4.30. IR (KBr, cm⁻¹): ν_{BH} = 2634, 2589, 2575, 2559, 2542, 2527, and 2513. Electronic spectrum (THF): 1170 (ε 680), 534 (ε 3000), and 370 nm (sh).

(B) Reaction of 6·PPN₂ with Excess FeCl₃. To a yellow slurry of **6·PPN₂** (106 mg, 0.0494 mmol) in CH₂Cl₂ was added an excess amount of FeCl₃ (140 mg, 0.86 mmol) in MeOH. Red-purple microcrystals were formed immediately. The reaction mixture was stirred for 4 h and filtered. The red-purple microcrystalline residue (40 mg, 0.037 mmol, 76%) was washed with 30 mL of MeOH (3 times), 10 mL of CH₂Cl₂ (3 times), and 10 mL of Et₂O (2 times) and dried by blowing N₂ over it. The same spectroscopic data were observed.

Reduction of 7·PPN. To a slurry of **7·PPN** (67 mg, 0.042 mmol) in 50 mL of THF was added an excess amount (18 mg, 0.46 mmol) of potassium. The reaction mixture was refluxed for 5 h, resulting in a yellow solution with yellow microcrystals. The residual potassium was removed mechanically, and an excess amount (300 mg, 0.522 mmol) of PPNCl was added. The reaction mixture was stirred for 14 h, and the resulting orange-yellow precipitate was collected, washed with 30 mL of THF and 30 mL of MeOH (2 times), and extracted with 10 mL of DMF. Pouring 50 mL of Et₂O into the DMF solution gave yellow microcrystals (64 mg, 0.030 mmol) of **6·PPN₂** in a yield of 72%.

Reduction of 8. (A) Reaction of 8 with Potassium. An excess amount of potassium (80 mg, 2.1 mmol) was added to a slurry of **8** (60 mg, 0.056 mmol) in 50 mL of THF. Refluxing of the solution caused the color to change to dark brown in 2 h and then to dark yellow. After 16 h of reflux, excess PPNCl (406 mg, 0.707 mmol) was added, and the reaction mixture was stirred for 4 h. 2-Propanol was added very slowly to the reaction mixture to quench the residual potassium until no evolution of gas was observed. The residual yellow precipitate was filtered, washed with 30 mL of MeOH, and then extracted with 15 mL of DMF. Precipitation by pouring 50 mL of Et₂O into the reaction mixture gave yellow microcrystals of **6·PPN₂** in a yield of 82% (98 mg, 0.046 mmol).

(B) Reaction of 8 with 6·PPN₂. 6·PPN₂ (107 mg, 0.0499 mmol) and **8** (54 mg, 0.051 mmol) were stirred in a mixed solvent of THF and CH₂Cl₂ (1:2). The mixture gradually turned brown, and after 2 h of stirring, all solvent was evaporated and the resulting dark brown residue was extracted with 20 mL of CH₂Cl₂. Pouring 60 mL of Et₂O into the reaction mixture gave black microcrystals of **7·PPN**. The black microcrystals (120 mg, 0.073 mmol, yield 74%) were washed with 10 mL of MeOH and 20 mL of Et₂O.

X-ray Structural Determination. Reflection data were collected on an Enraf-Nonius CAD4TSB diffractometer with graphite-mono-chromated Mo Kα radition (λ = 0.71073 Å) at 20 °C. The accurate

cell parameters and the orientation matrixes were determined from the least-squares fit of 25 accurately centered reflections. Data were collected with the ω/2θ scan mode for **2·PPN₂** and **3·PPN**, ω scan mode for **4**, and ω/θ scan mode for **6·PPN₂**, **7·PPN**, and **8**. The data were corrected for Lorentz-polarization effects, and ψ-scan absorption correction was applied. The structures of the compounds were solved by Patterson's heavy atom method (SHELXS-86).[16] Non-hydrogen atoms except C1′ of **3·PPN**, which was refined isotropically, were refined by full-matrix least-squares techniques (SHELXL-93)[17] with anisotropic displacement parameters. Phenyl hydrogens were placed at their geometrically calculated positions (d_{CH} = 0.930 Å) and refined riding on the corresponding carbon atoms with isotropic thermal parameters (U = 1.2U(C$_{phenyl}$)). Carboranyl hydrogens were refined isotropically for **2·PPN₂**, **6·PPN₂**, and **7·PPN** (except cage C–H) or placed at their geometrically calculated positions ($d_{C(or\ B)H}$ = 1.10 Å) and refined riding on the corresponding carbon atoms with isotropic thermal parameters (U = 1.2U(C(or B)$_{carboranyl}$)) for the remaining compounds. Crystallographic data are given in Table 1.

Physical Measurements. Infrared spectra were measured as KBr pellets on a Bomem MB-100 FTIR spectrometer. ¹H NMR spectra were obtained at 300.13 MHz on a Bruker AM 300 spectrometer and were referenced to internal solvent peaks. ¹¹B NMR spectra were recorded at 96.295 MHz on a Bruker AM 300 instrument and referenced to external BF₃·OEt₂. All chemical shifts downfield of the reference are designated as positive. Korea Basic Science Institute, Seoul Branch, Korea, provided the elemental analyses for C, H, and N. The electronic absorption spectra were recorded on a Shimadzu UV-3100S spectro-photometer. The magnetic susceptibilities of powdered samples were measured by using a Johnson-Matthey magnetic susceptibility balance calibrated with HgCo(NCS)₄.[18] The experimental magnetic susceptibility data were corrected for the diamagnetism of constituent atoms by using Pascal's constants.[19] Cyclic voltammetry was conducted in THF or DMF containing 0.1 M n-Bu₄NPF₆ as a supporting electrolyte with platinum wires as working and counter electrodes and a Ag/AgCl reference electrode. Potentials were determined by using a homemade electro-chemical analyzer at scan rate 40 mV/s and referenced to the ferrocene/ferrocenium couple employed as a standard in DMF or THF. X-ray photoelectron spectra (XPS) were obtained by using a VG-ESCALAB 200-i instrument using Al Kα exciting radiation at ambient temperature and pressures less than 10⁻⁹ Torr. The energy scale was calibrated by emission from the Ag 3d$_{5/2}$ line at 368.3 eV. The photon resolution was 0.8 eV at 1486 eV photon energies. All solid samples were introduced into the analysis chamber after the sample surface was cleaned with a scraper. Spectra were deconvoluted with a Gaussian–Lorentzian line shape using a nonlinear least-squares procedures.

Results and Discussion

Synthesis and Structure. The synthetic routes to two novel families of three-component reversible redox cycles of dinuclear molybda- and tungstacarboranes are outlined in Schemes 1 and 2, respectively.

[(C₂B₉H₁₁)M(μ-SPh)₂]₂·PPN₂ (M = Mo, 2·PPN₂ and W, 6·PPN₂), Systems Involving the Scission of the C–C Cluster Bond. Refluxing [(C₂B₉H₁₁)M(CO)₃]·PPN₂ (M = Mo, **1·PPN₂** and W, **5·PPN₂**) in the presence of an excess amount of phenyl disulfide (PhSSPh) gave PPN salts of the completely decarbo-nylated dinuclear anion species **2** and **6**. Since the addition of 1 equiv of PhSSPh to **1·PPN₂** is known to give the partially decarbonylated product [(C₂B₉H₁₁)Mo(SPh)₂(CO)₂]·PPN₂,[20]

(16) Sheldrick, G. M. SHELXS-86 *User Guides*; Crystallographic Department, University of Göttinggen, Germany, 1985.

(17) Sheldrick, G. M. SHELXL-93 *User Guides*; Crystallographic Department, University of Göttinggen, Germany, 1993.

(18) Brown, D. B.; Crawford, V. H.; Hall, J. W.; Hatfield, W. E. *Phys. Chem.* **1977**, *81*, 1303.

(19) (a) Figgis, B. N.; Lewis, J. *Modern Coordination Chemistry*; Interscience: New York, 1960; Chapter 6, p 403. (b) Konig, E. *Magnetic Properties of Transition Metal Compounds*; Springer-Verlag: West Berlin, 1966. (c) Wellar, R. R.; Hatfield, W. E. *J. Chem. Educ.* **1980**, *19*, 1095.

(20) Kim, J.-H.; Hong, E.; Kim J.; Do, Y. *Inorg. Chem.* **1996**, *35*, 5112.

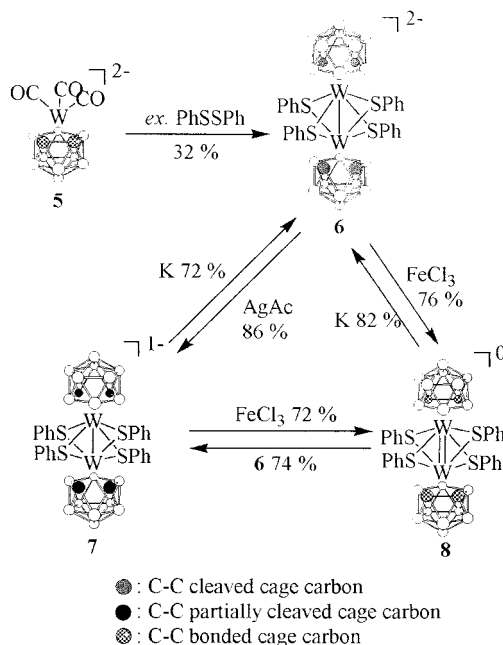**Table 1.** Crystallographic Data for **2**·PPN$_2$, **3**·PPN, **4**, **6**·PPN$_2$, **7**·PPN, and **8**

	2·PPN$_2$	**3**·PPN	**4**	**6**·PPN$_2$	**7**·PPN	**8**
formula	[C$_{50}$H$_{51}$NB$_9$P$_2$S$_2$Mo]$_2$	C$_{64}$H$_{72}$NB$_{18}$P$_2$S$_4$Mo$_2$	[C$_{14}$H$_{21}$B$_9$S$_2$Mo]$_2$	[C$_{50}$H$_{51}$NB$_9$P$_2$S$_2$W]$_2$	C$_{64}$H$_{72}$NB$_{18}$P$_2$S$_4$W$_2$	[C$_{14}$H$_{21}$B$_9$S$_2$W]$_2$
FW	1970.42	1431.87	893.32	2146.24	1607.69	1069.14
radiation source	MoKα	MoKα	MoKα	MoKα	MoKα	MoKα
wavelength (Å)	0.71073	0.71073	0.71073	0.71073	0.71073	0.71073
crystal system	monoclinic	triclinic	monoclinic	monoclinic	triclinic	monoclinic
color of crystal	yellow-orange	black	green	yellow-orange	black	purple
space group	$P12_1/c1$	$P\bar{1}$	$P12_1/c1$	$P12_1/c1$	$P\bar{1}$	$P12_1/c1$
a (Å)	12.728(5)	13.060(2)	10.150(1)	12.695(2)	12.999(6)	10.176(1)
b (Å)	14.436(1)	13.061(2)	16.296(3)	14.482(2)	13.015(5)	16.361(3)
c (Å)	26.462(4)	21.782(4)	11.762(3)	26.561(7)	21.889(9)	11.783(5)
α (deg)	90	74.645(15)	90	90	75.10(3)	90
β (deg)	90.39(2)	74.575(15)	98.023(9)	90.64(2)	75.08(4)	98.03(2)
γ (deg)	90	82.118(15)	90	90	82.18(4)	90
V (Å^3)	4862.3(19)	3444.9(11)	1926.5(6)	4883.0(16)	3448.5(26)	1942.5(9)
Z	2	2	2	2	2	2
d_{calc} (g/cm^3)	1.346	1.380	1.540	1.460	1.548	1.828
μ (mm^{-1})	0.458	0.573	0.892	2.553	3.542	6.156
$F(000)$	2028	1462	896	2156	1590	1024
2θ range (deg)	$4 \le 2\theta \le 50$	$4 \le 2\theta \le 50$	$4 \le 2\theta \le 50$	$4 \le 2\theta \le 50$	$4 \le 2\theta \le 50$	$4 \le 2\theta \le 48$
h	$0 \le h \le 15$	$0 \le h \le 10$	$0 \le h \le 12$	$0 \le h \le 15$	$-15 \le h \le 15$	$0 \le h \le 11$
k	$0 \le k \le 17$	$-15 \le k \le 15$	$0 \le k \le 19$	$0 \le k \le 17$	$0 \le k \le 15$	$0 \le k \le 18$
l	$-31 \le l \le 31$	$-24 \le l \le 25$	$-13 \le l \le 13$	$-31 \le l \le 31$	$-25 \le l \le 26$	$-13 \le l \le 13$
no. of indep rflns	7287	8281	2813	7750	10 976	2794
no. of obsd rflns ($|F_o| > 4\sigma(F_o)$)	5800	5969	1994	6883	8996	2375
no. of params refined	534	695	211	534	772	211
$R_1{}^a$ ($|F_o| > 4\sigma(F_o)$)	0.0434	0.0690	0.0556	0.0337	0.0387	0.0360
$wR_2{}^a$ ($|F_o| > 4\sigma(F_o)$)	0.0970	0.1890	0.0984	0.1022	0.0827	0.0993
GOF ($|F_o| > 4\sigma(F_o)$)	1.026	1.083	1.104	1.021	1.072	1.167
x	0.0515	0.1421	0.0426	0.0739	0.0325	0.0568
y	5.1327	2.0825	0.0000	9.2810	8.1699	0.0000

^{a} $R_1 = \sum ||F_o| - |F_c||/\sum |F_o|$. ^{b} $wR_2 = [\sum[w(F_o{}^2 - F_c{}^2)^2]/\sum[w(F_o{}^2)^2]]^{1/2}$, where $w = 1/[\sigma^2(F_o{}^2) + (xP)^2 + yP]$, $P = (F_o{}^2 + 2F_c{}^2)/3$.

Scheme 1. Synthesis of **2**, **3**, and **4**

Scheme 2. Synthesis of **6**, **7**, and **8**
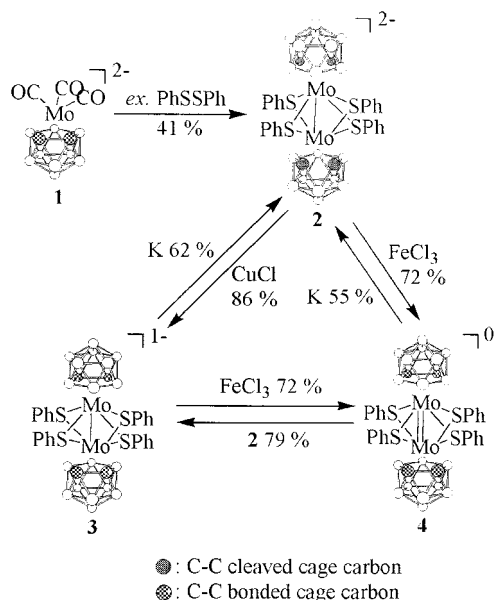
it seems that [(C$_2$B$_9$H$_{11}$)M(SPh)$_2$(CO)$_2$]·PPN$_2$ (M = Mo and W) are the intermediates in the formation of **2**·PPN$_2$ and **6**·PPN$_2$.

The structures of the two complexes, as shown in Figure 1, are isostructural and isomorphous. Both dianions are discrete dimers oriented about the crystallographic inversion centers lying in the middle of M–M bonds. Four bridging thiolate groups are arranged such that the two planar MSMS rhombi are perpendicular to each other, the MS1M′S1′ plane bisects

the cage C···C vector, and the overall symmetry lacks a mirror plane. Analysis of the interatomic distances in Table 2 reveals that the carborane cages show a striking feature of scission ("switch off") of the C1–C2 cluster bond (C1···C2 distance of 2.560 Å in **2**·PPN$_2$ and 2.600 Å in **6**·PPN$_2$) with concomitant movement of B6 toward the metal center (M···B6 2.894 Å in **2**·PPN$_2$ and 2.849 Å in **6**·PPN$_2$), which can be described as a DSD process.

Table 2.   Selected Interatomic Distances (Å) and Angles (deg) of **2·PPN₂**, **3·PPN**, **4**, **6·PPN₂**, **7·PPN**, and **8**

	2·PPN₂	3·PPN	4	6·PPN₂	7·PPN	8
M3−M3′	2.8153(12)	2.7251(13)	2.7103(12)	2.8383(8)	2.7700(13)	2.7331(13)
M3−S1	2.5330(15)	2.485(3)	2.468(2)	2.5374(15)	2.501(2)	2.467(3)
M3−S2	2.5178(15)	2.466(3)	2.474(2)	2.5372(15)	2.506(2)	2.479(3)
M3−S1′	2.5101(15)	2.453(3)	2.458(2)	2.5093(15)	2.475(2)	2.462(3)
M3−S2′	2.4983(14)	2.448(2)	2.461(2)	2.5204(15)	2.4944(19)	2.460(2)
M3−C1	2.176(4)	2.337(11)	2.341(7)	2.154(5)	2.220(8)	2.353(10)
M3−C2	2.161(5)	2.311(12)	2.319(8)	2.149(5)	2.220(8)	2.322(10)
M3−B7	2.374(5)	2.392(11)	2.355(9)	2.347(6)	2.371(8)	2.358(11)
M3−B8	2.426(6)	2.451(16)	2.412(10)	2.421(7)	2.409(8)	2.395(12)
M3−B4	2.381(5)	2.400(13)	2.401(8)	2.377(6)	2.355(10)	2.401(11)
C1−C2	2.560(6)	1.663(15)	1.581(11)	2.600(8)	2.170(13)	1.605(14)
C2−B7	1.607(7)	1.717(18)	1.703(12)	1.640(8)	1.665(12)	1.710(15)
B7−B8	1.817(8)	1.79(2)	1.785(13)	1.782(10)	1.784(12)	1.793(17)
B8−B4	1.789(8)	1.788(19)	1.813(12)	1.787(10)	1.763(12)	1.827(17)
B4−C1	1.602(7)	1.649(19)	1.699(11)	1.639(8)	1.582(15)	1.699(14)
M−B6	2.894(5)			2.849(6)	3.223(13)	
C1−M3−C2	72.34(17)	41.9(4)	39.7(3)	74.4(2)	58.5(3)	40.1(3)
M3−S1−M3′	67.87(3)	66.98(8)	66.76(6)	68.44(4)	67.64(6)	67.35(6)
M3−S2−M3′	68.28(3)	67.36(7)	66.63(5)	68.28(4)	67.27(6)	67.20(6)
C1−B6−C2	96.5(3)	56.7(7)	54.3(5)	97.7(4)	80.0(7)	54.8(6)
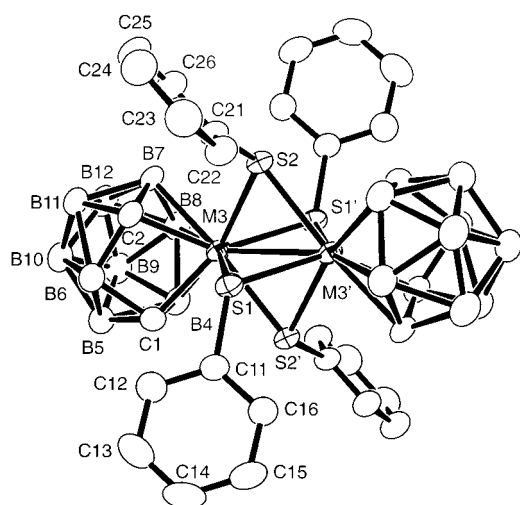
Figure 1. ORTEP drawing of **2** showing 50% probability thermal ellipsoids. Isostructural **6** has a similar perspective view with the same numbering scheme. All hydrogen atoms have been omitted for clarity.

Both compounds also have the same structural integrity in solution, as shown by NMR spectroscopy. The ¹¹B{¹H} NMR spectra of **2·PPN₂** and **6·PPN₂** in DMSO-d_6 at room temperature are rather featureless due to the broad band character. But the ¹H NMR spectra show two well-resolved singlets with equal intensity assignable to the carboranyl CH protons of the C₂B₉ cage, being consistent with the absence of a mirror plane. In addition, the ¹H−¹H coupling peaks of the carboranyl CH protons in both cases are not observed in the ¹H homonuclear two-dimensional COSY spectra (Supporting Information), which is in good agreement with the scission of C1···C2 bonds observed in the X-ray structure.

Although the deformed C₂B₉M frameworks of **2** and **6** resemble the pseudocloso framework or the hypercloso framework, these systems cannot be classified either by the pseudocloso framework or by the hypercloso framework. The pseudocloso metallacarborane cluster,[8] which no longer shows the closo geometry because of the cleaved nature of the cage C−C bond but obeys the Wade's rules[21] and has an 18-electron metal center, has its C−C bond cleavage origin in the steric crowding introduced to both cage carbon atoms while the hypercloso metallacarborane, suggested by Hawthorne et al.[5] and Baker,[22]

alternatively referred to as the isocloso framework by Kennedy,[23] has its C−C bond cleavage origin in the unsaturation of the metal center as 16 electrons. Therefore, the lack of bulky substituents at the cage carbon atoms and the saturation of the metal centers by 18 electrons in **2** and **6** exclude the possibility of classifying them as either the pseudocloso framework or the hypercloso system. In other words, the origin of the cage C−C bond cleavage for **2** and **6** is different from the steric crowding and the unsaturation of the metal center, indicating that these systems represent a new type of deformed cage, the semicloso framework. The driving force for the semicloso framework is the intramolecular redox reaction between the carborane cage and the metal center as supported by the XPS experiments (vide infra).

[(C₂B₉H₁₁)M(μ-SPh)₂]₂·PPN (M = Mo, 3·PPN and W, 7· PPN), Systems Involving the Re-formation of the C−C Cluster Bond. One-electron oxidation of **2·PPN₂** with CuCl gives [(C₂B₉H₁₁)Mo(μ-SPh)₂]₂·PPN (**3·PPN**) in good yield (86%). The X-ray diffraction study reveals that the asymmetric unit consists of two half-fragments of an anion and one PPN cation. Each of the two fragments gives a complete dinuclear monoanion by inversion operation. One of the two anions is shown in Figure 2, and the selected interatomic distances and angles are listed in Table 2. The room-temperature solid-state magnetic moment measurement for **3·PPN**, which yielded an effective magnetic moment of 1.70 μ_B, indicates the presence of an unpaired electron as expected for a mixed-valence complex. The C₂B₉Mo cluster in **3·PPN** shows a typical feature of a closo C₂B₉M framework with the C−C distance of 1.663 Å. The structural comparison of **3·PPN** with **2·PPN₂** reveals the re-formation of the cage C−C bond ("switch on") during the oxidation process. In other words, the "switch off → switch on" conversion, or the semicloso → closo cage conversion, occurs during the *one-electron oxidation process* without accompanying the structural change in the complex backbone.

It is worthy to note that the hypercloso → closo cage conversion was observed for the 12-vertex hypercloso C₂B₉W framework systems[6,7] as well as in the RuC₂B₇[5] and IrB₉ frameworks.[24] For the 12-vertex hypercloso C₂B₉W framework systems, the conversion, usually accompanied by the change

(21) Wade, K. *Chem. Commun.* **1971**, 792.

(22) Kennedy, J. D. *Inorg. Chem.* **1986**, *25*, 111.

(23) Baker, R. T. *Inorg. Chem.* **1986**, *25*, 109.

(24) Coldicott, R. S.; Kennedy, J. D.; Thornton-Pett, M. *J. Chem. Soc., Dalton Trans.* **1996**, 3819.
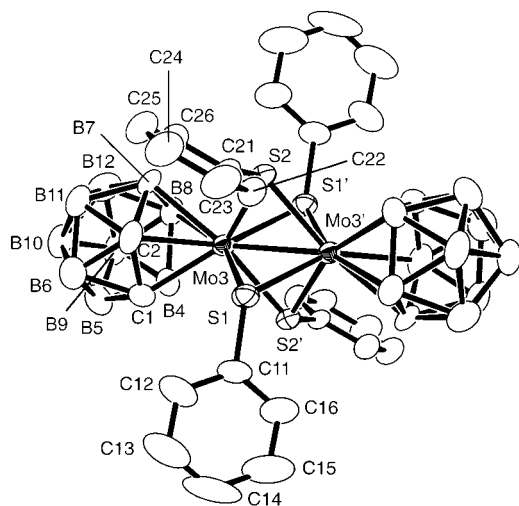
Figure 2. ORTEP drawing of **3** showing 50% probability thermal ellipsoids. All hydrogen atoms have been omitted for clarity.
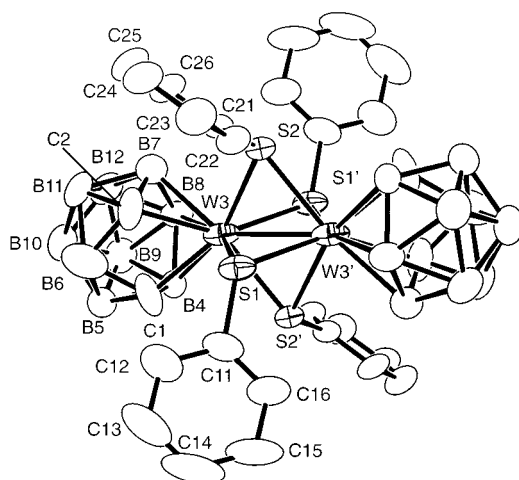

Figure 3. ORTEP drawing of **7** showing 50% probability thermal ellipsoids. All hydrogen atoms have been omitted for clarity.

Figure 4. ORTEP drawing of **4** showing 50% probability thermal ellipsoids. Isostructural **8** has a similar perspective view with the same numbering scheme. All hydrogen atoms have been omitted for clarity.

in the complex backbone, was driven by equimolar reaction with two electron donors, PMe_3 and $CNBu^t$, at room temperature, reflecting the electron deficiency of the metal center of the hypercloso framework. In this regard, the lack of the reactivity of **2** toward donor molecules PMe_3 and $CNBu^t$, even at the 85 °C for 1 week, and its conversion to the closo system upon one-electron oxidation support that it is not a hypercloso system.

The "switch off → switch on" process is shown to be reversible: Reduction of **3**·PPN by reacting with potassium followed by cation exchange with PPNCl leads to the cage C—C cleaved ("switch off") **2**·PPN_2 in moderate yield (62%). This constitutes the first example of the reversible "switch off ↔ switch on" process driven by one-electron redox reactions in the metallacarborane system.[25]

In contrast to the complete re-formation of the cage C—C bond in **3**·PPN, its tungsten analogue $[(C_2B_9H_{11})W(\mu\text{-}SPh)_2]_2$·PPN (**7**·PPN), synthesized by one-electron oxidation of **6**·PPN_2 using silver acetate as an oxidant, shows the partial re-formation of the cage C—C bond. The molecular structure of **7** (Figure 3), which shows a dinuclear nature oriented about a crystallographic inversion center, is similar to that of **3**, except that

the C_2B_9W cage shows deformation with the C1—C2 distance being 2.170 Å. This value falls between those in **2** (2.560 Å) and **3** (1.663 Å), suggesting the possibility of **7** being an intermediate state in the process of "switch off → switch on". The cage with the similar deformation has only been observed in the pseudocloso frameworks $[1,2\text{-}(SPh)_2\text{-}3\text{-}(p\text{-cymene})\text{-}3,1,2\text{-}Ru\text{-}C_2B_9H_9]$[26] (C1—C2 2.107 Å) and $[1\text{-}(PhCC)\text{-}2\text{-}Ph\text{-}3\text{-}(p\text{-cymene})\text{-}3,1,2\text{-}RuC_2B_9H_9]$[8] (C1—C2 2.187 Å), where the cage C—C distance can be adjusted by controlling the steric effects of the substituents. The different ν_{BH} patterns in IR spectra of **7**·PPN and **3**·PPN are also indicative of the presence of the different cage geometry in each compound in the solid state. The $^1H–^1H$ COSY study that can confirm the cage C—C cleavage of **7**·PPN was hampered by the paramagnetism (μ_{eff} = 1.80 μ_B) of the compound.

$[(C_2B_9H_{11})M(\mu\text{-}SPh)_2]_2$ (M = Mo, 4 and W, 8), Systems with the Typical Closo Frameworks. Two-electron oxidation of **2**·PPN_2 and **6**·PPN_2 or one-electron oxidation of **3**·PPN and **7**·PPN gave the neutral species $[(C_2B_9H_{11})M(\mu\text{-}SPh)_2]_2$ (M = Mo, **4**; W, **8**), respectively. The green **4** and the red-purple **8** show extremely low solubility in most common solvents (only slightly soluble in THF), hampering the purification and the growth of single crystals. The best way to get them in pure form is slow diffusion of a solution of $FeCl_3$ in MeOH to a solution of **3**·PPN (or **7**·PPN) in CH_2Cl_2, followed by repeated washing with CH_2Cl_2 (to remove any residual **3**·PPN (or **7**·PPN)) and MeOH (to remove residual $FeCl_3$ and byproduct PPNCl and $FeCl_2$). Single crystals suitable for X-ray studies were also obtained by this method.

The X-ray structures of **4** and **8** (Figure 4) are isostructural and isomorphous. The C_2B_9M clusters show the typical closo nature with the cage C1—C2 bond of 1.581 Å for **4** and 1.605 Å for **8** (Table 2). The complete re-formation of the cage C—C bond in **8** is interesting since its one-electron-reduced species, **7**·PPN, shows an intermediate C—C cleaved feature. The observed trends in the "switch off → switch on" processes involved in two novel families of three-component reversible redox cycles $[(C_2B_9H_{11})M(\mu\text{-}SPh)_2]_2^n$ (M = Mo, W; n = 2−, 1−, 0) indicate that the increased oxidation state of the metals and thereby the increased electronegativity of the metal centers

(25) Recently, the reversible and quantitative interconversion of hypercloso ↔ closo by *electronic redox* reaction has been reported in the metallaborane system. See: Littger, R.; Englich, U.; Ruhlandt-Senge, K.; Spencer, J. T. *Angew. Chem., Int. Ed.* **2000**, *39*, 1472.
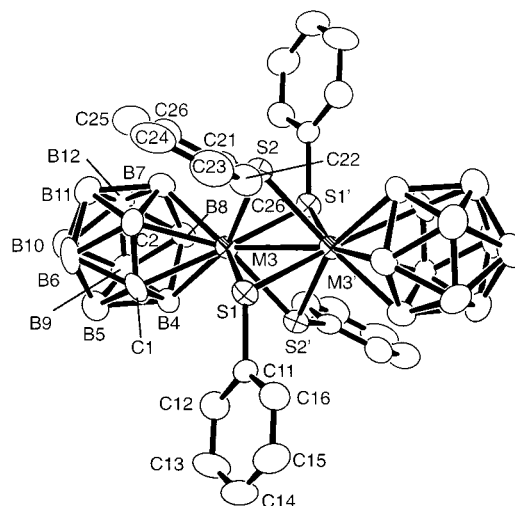
(26) Teixidor, F.; Viñas, C.; Flores, M. A.; Rosair, G. M.; Welch, A. J.; Weller, A. S. *Inorg. Chem.* **1998**, *37*, 5394.

lead to the restoration of the closo nature of the cage. The detailed electronic effect is discussed below with the XPS results.

One-electron and two-electron reductions of **4** have also been accomplished, completing the reversible chemical redox cycle as shown in Scheme 1. The reaction of **4** with potassium followed by cation exchange with PPNCl gave the two-electron-reduced product **2·PPN$_2$** in moderate yield (55%). Reacting **4** with **2·PPN$_2$** gave the one-electron-reduced product **3·PPN** in good yield (79%). As shown in Scheme 2, the family of dinuclear tungstacarboranes also forms a complete reversible chemical redox cycle, constituting the example of the unprecedented reversible C—C cleavage (**6·PPN$_2$**) ↔ C···C intermediate state (**7·PPN**) ↔ C—C formation (**8**) process.

M—M and M—S Distances. It is well known that in the angularly strained-bridged systems, the bridging ligands effectively elongate the M—M distance.[27] But the M—M distances in the systems reported in this paper are even significantly longer than the reported values of the analogous complexes: **2·PPN$_2$** (2.8153 Å) and **6·PPN$_2$** (2.8383 Å) vs [Mo(η^5-C$_5$H$_5$)(SCH$_3$)$_2$]$_2$ (2.603 Å)[27] and [Mo(η^6-PhCH$_3$)(μ-SCH$_3$)$_2$]$_2$$^{2+}$ (2.614 Å),[28] **3** (2.7251 Å) and **7** (2.7700 Å) vs [Mo(η^5-C$_5$H$_5$)(SCH$_3$)$_2$]$_2$·PF$_6$ (2.617 Å),[27] and **4** (2.7103 Å) and **8** (2.7331 Å) vs [(CpMo)$_2$-(μ-S)(μ-SCH$_3$)S$_2$CH$_2$]$^+$ (2.610 Å)[29] and [Cp$_2$Mo$_2$(μ-S)(μ-Te)-(μ-SPh)$_2$] (2.635 Å).[30] This elongation is probably due to the steric interactions between the cages and the thiolate phenyl rings, as judged by the shortest H$_{cage}$–H$_{phenyl}$ distances in the complexes: 2.140 Å for H7–H16′ in **2**, 2.113 Å (2.097 Å in molecule B) for H7–H16′ in **3**, 2.101 Å for H2–H26 in **4**, 2.192 Å for H7–H16′ in **6**, 2.082 Å (2.152 Å for molecule B) for H7–H16′ in **7**, and 2.090 Å for H2–H26 in **8**.

The comparison of the difference in M—M distances between the molybdenum and tungsten analogues also indicates that the cleavage of the cage C—C bond leads to the increase in the steric interactions via the increase in the cage size and thus to the elongation of the M—M distance. The difference in M—M distances between **2** and **6** or **4** and **8**, where molybdenum and tungsten analogues show the same cage geometry, is 0.023 Å, which is in good agreement with twice the ionic radius difference of 0.01 Å between Mo(IV) (0.65 Å) and W(IV) (0.66 Å).[31] The difference in M—M distances between **3** and **7**, where the molybdenum analogue has a closo cage and the tungsten analogue has a deformed cage, is 0.045 Å, which is larger than in the cases above.

The M—S distance also seems to be affected by the steric congestion. Although the average M—S distances in **3·PPN** (2.463 Å), **4** (2.465 Å), and **8** (2.467 Å), where the carborane cages show the closo feature, are similar to those in [Mo(η^5-C$_5$H$_5$)(SCH$_3$)$_2$]$_2$ (2.46 Å),[27] [Mo(η^5-C$_5$H$_5$)(SCH$_3$)$_2$]$_2$·PF$_6$ (2.44 Å),[27] and [Mo(η^6-PhCH$_3$)(μ-SCH$_3$)$_2$]$_2$$^{2+}$ (2.451−2.462 Å),[28] the M—S distances in **2·PPN$_2$** (2.5148 Å) and **6·PPN$_2$** (2.5261 Å), where the cages show significant distortion, are significantly longer than the others, and the M—S distance (2.494 Å) in the intermediately distorted **7·PPN** is slightly longer than those in the closo complexes.

The paramagnetism of **4** and **8** can be also explained in terms of the M—M bond elongation. Formally, the metals in **4** and **8**
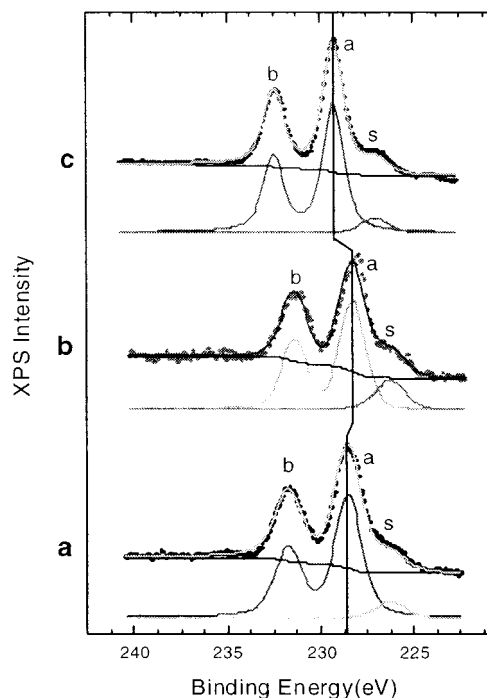
(27) Connelly, N. G.; Dalh, L. F. *J. Am. Chem. Soc.* **1970**, *92*, 7470.
(28) Silverthorn, W. E.; Couldwell, C.; Prout, K. *Chem. Commun.* **1978**, 1009.
(29) Casewit, C. J.; Haltiwanger, R. C.; Noordik, J.; DuBois, M. R. *Organometallics* **1985**, *4*, 119.
(30) Mathur, P.; Ghose, S.; Trivedi, R.; Gelinsky, M.; Rombach, M.; Vahrenkamp, H.; Banerjee, S.; Philip, R.; Kumar, G. R. *J. Organomet. Chem.* **2000**, *595*, 140.
(31) Greenwood, N. N.; Earnshow, A. *Chemistry of the Elements*; Pergamon Press: New York, 1984; p 1170.

Figure 5. X-ray photoelectron spectra of (a) **2·PPN$_2$**, (b) **3·PPN**, and (c) **4**. The label a is assigned to the values of Mo 3d$_{5/2}$, the label b is assigned to the value of Mo 3d$_{3/2}$, and the label s is assigned to the value of S 2p of the three complexes.

Table 3.   XPS Results for **2·PPN$_2$**, **3·PPN**, and **4**

	Mo 3d$_{3/2}$ (eV)^a	Mo 3d$_{5/2}$ (eV)^b	FO^c	EO^d	EC^e
2·PPN$_2$	231.7	228.5	(3, 3)	(3.6,3,6)	(−2.6,−2.6)
3·PPN	231.4	228.3	(3, 4)	(3.5,3.5)	(−2,−2)
4	232.5	229.3	(4, 4)	(4,4)	(−2,−2)

^{a} Mo 3d$_{3/2}$ is the core electron binding energy of the Mo 3d$_{3/2}$ level. ^{b} Mo 3d$_{5/2}$ is the core electron binding energy of the Mo 3d$_{5/2}$ level. ^{c} FO is the formal oxidation state of the metal. ^{d} EO is the effective oxidation state of the metal. ^{e} EC is the effective charge of the carborane cage.

have oxidation states of IV−IV and thus the d^2−d^2 configuration. The electron count of both complexes then leads to double bond character for the M—M bonds, so diamagnetism should result. But **4** and **8** show weak paramagnetism of μ_{eff} = 1.6 and 1.5 μ_B, respectively. This is probably due to the fact that a molecular triplet state could arise by the elongation of the double M—M bond, leaving a single electron on each metal that then could couple through a weak antiferromagnetic exchange mechanism. A similar observation has been reported in [(η^5-C$_5$H$_5$)V(SMe)$_2$]$_2$.[32]

Origin of the Cleavage and Formation of the Cage C—C Bond. The reversible "switch off ↔ switch on" conversions in molybda- and tungstacarborane systems occur during the redox processes without causing any significant structural change in the complex backbone, suggesting that the cleavage and formation of the cage C—C bond is affected purely by the electronic effect. To probe the origin of the cleavage and formation of the cage C—C bond, the XPS studies were performed.

Molybdacarboranes. Shown in Figure 5 and Table 3 are the X-ray photoelectron spectra and the binding energies for the molybdenum systems, respectively. The binding energy

(32) Holm, R. H.; King, R. B.; Stone, F. G. A. *Inorg. Chem.* **1963**, *2*, 219.

Three-Component Reversible Redox Cycles

J. Am. Chem. Soc., Vol. 123, No. 37, 2001 9061

increases in the order of **3·PPN** < **2·PPN$_2$** < **4**, indicating that the electron density of the metal decreases in that order and thus the "effective oxidation state"[33] of the metal increases in that order. This observation is rather surprising since the formal oxidation state of the metal (Table 3) is expected to increase in the order of **2·PPN$_2$** < **3·PPN** < **4** based on the use of the progressive oxidation condition in the synthesis of **3·PPN** from **2·PPN$_2$** and **4** from **3·PPN** (Scheme 1). The "effective oxidation state" of the metal center was estimated from the observed binding energy data and summarized in Table 3. (The details of the XPS interpretation are deposited as Supporting Information.) Since no cage deformation is observed in **3·PPN** and **4**, their formal oxidation states were taken as the "effective oxidation states". The "effective charge"[34] of the carborane cage, also listed in Table 3, was then obtained assuming the bridging thiolates remain uninvolved in the intramolecular competition for the charge. For **2·PPN$_2$**, the oxidation state of the metal changed from the formal value of 3 to the effective value of 3.6, and the "effective charge" of the carborane cage became -2.6 from -2 with concomitant change in the C–C bond distance. Therefore, the intramolecular redox reaction or the intramolecular reduction of the cage that occurred in **2·PPN$_2$** can be considered as the origin of the cleavage of the cage C–C bond.

It is known that the intermolecular reduction the *o*-carborane gives the dianion *nido*-C$_2$B$_{10}$H$_{12}{}^{2-}$ that interacts with metal in the η^6 mode,[10] and further reduction even leads to the tetraanion *arachno*-C$_2$B$_{10}$H$_{12}{}^{4-}$ that interacts with the metal in the η^7 mode.[11] Both anions have the cleaved feature in the C–C cage bond. It is also interesting to note that withdrawing electron density from the electronically saturated metal center to the cage drives the cage deformation in **2·PPN$_2$**, but the cage in the hypercloso system deforms to resolve the electron deficiency of the electronically unsaturated metal center.[35]

The conversion to the closo framework during oxidation process also deserves explanation: As oxidation occurs, the formal oxidation state of the Mo atom increases (**2·PPN$_2$**(III,-III) → **3·PPN**(III,IV)), resulting in more electronegative metal centers. So, the electronegativity of the metals in **3·PPN** is large enough to win the competition of electron density with respect to the carborane cage. To our knowledge, this kind of "competition" of electron density between the metal and the ligand that can lead to the reversible structural change has never been reported before. If further oxidation occurs to give **4** in the formal oxidation state of (IV,IV), the metal center is even more electronegative and does not lose electron density to the carborane cage, resulting in the closo cage.

Tungstacarboranes. The XPS study of the tungsten analogues, summarized in Figure 6 and Table 4, reveals the importance of the relative electronegativity of the metal compared to the cage in determining the cage structures of tungstacarboranes. Listed also in Table 4 are the "effective oxidation state" of the metals and the "effective charge" of the carborane cages in the tungsten systems that were estimated analogously to the molybdenum systems on the basis of the following approximations: Since the distortion of the cage in **6·PPN$_2$** (C1···C2 2.600 Å) is very similar to that in **2·PPN$_2$** (C1···C2 2.560 Å), the "effective charge" of the carborane cages

(33) The "effective oxidation state" is a relative value of the electron density of the metal center in the scale of formal oxidation state.

(34) The "effective charge" is a relative value of the electron density of the carborane cage. It is given as the following: (the formal oxidation state of the metal center) − (the effective oxidation state of the metal center) + (the formal charge of the carborane cage, 2−).

(35) Johnston, R. L.; Mingos, D. M. P.; Sherwood, P. *New J. Chem.* **1991**, *15*, 831.
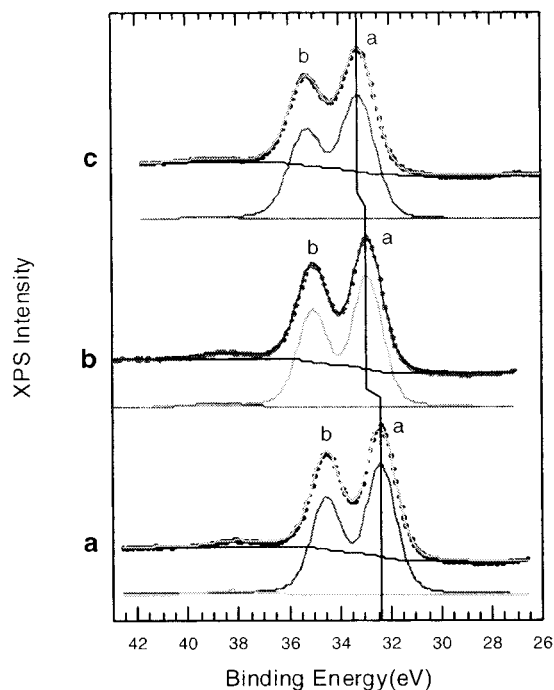

Figure 6. X-ray photoelectron spectra of (a) **6·PPN$_2$**, (b) **7·PPN**, and (c) **8**. The label a is assigned to the values of W 4f$_{7/2}$, and the label b is assigned to the value of W 4f$_{5/2}$ of the three complexes.

Table 4. XPS Results for **6·PPN$_2$**, **7·PPN**, and **8**

	W 4f$_{5/2}$ (eV)^a	W 4f$_{7/2}$ (eV)^b	FO^c	EO^d	EC^e
6·PPN$_2$	34.5	32.4	(3,3)	(3.6,3.6)	(−2.6,−2.6)
7·PPN	35.0	32.9	(3,4)	(3.85,3.85)	(−2.35,−2.35)
8	35.2	33.2	(4,4)	(4,4)	(−2,−2)

^{a} W 4f$_{5/2}$ is the core electron binding energy of the W 4f$_{5/2}$ level. ^{b} W 4f$_{7/2}$ is the core electron binding energy of the W 4f$_{7/2}$ level. ^{c,d,e} Definitions are the same as those given in the footnotes of Table 3.

in **6·PPN$_2$** was taken as 3.6. In addition, the formal and effective oxidation states of **8** were considered unchanged because the carborane cage in **8** shows no deformation.

The values in Table 4 show that the increasing trend of the binding energy in the order of **6·PPN$_2$** < **7·PPN** < **8** is consistent with their increasing trend in the "effective oxidation state" of the metal. The decreasing trend of the extent of the cage deformation in the order of **6·PPN$_2$** > **7·PPN** > **8** is also in accord with their decreasing trend in the "effective charge" of the cage. The "effective oxidation state" of 3.85 for the metal center in **7·PPN** gave the "effective charge" of -2.35 for the cage. Because of this reduced nature of the cage, the cage deformation still exists in **7·PPN**. The plot of the "excessive charge" of the cage[36] vs the cage C–C distance for the tungsten systems, given in Figure 7, shows a linear relationship, suggesting that the cage C–C distance, which represents the extent of deformation, is proportional to the excessive charge of the cage.

It is important to note the difference in the structures of **3·PPN** and **7·PPN**, the closo cage for the former and the intermediately deformed cage for the latter. This difference is presumably due to the difference in electronegativity of the metal atom (W, 1.7; Mo, 1.8).[31] The intermediate deformation of the cage in **7·PPN** suggests that the compound is at the borderline

(36) The "excessive charge" is the difference between the formal charge and the "effective charge" of the carborane cage.
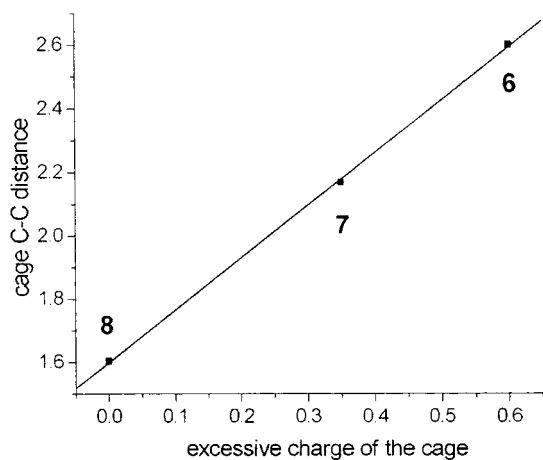
Figure 7. Plot of the excessive charge of the cages vs the cage C−C distances (Å) for the tungstacarboranes.
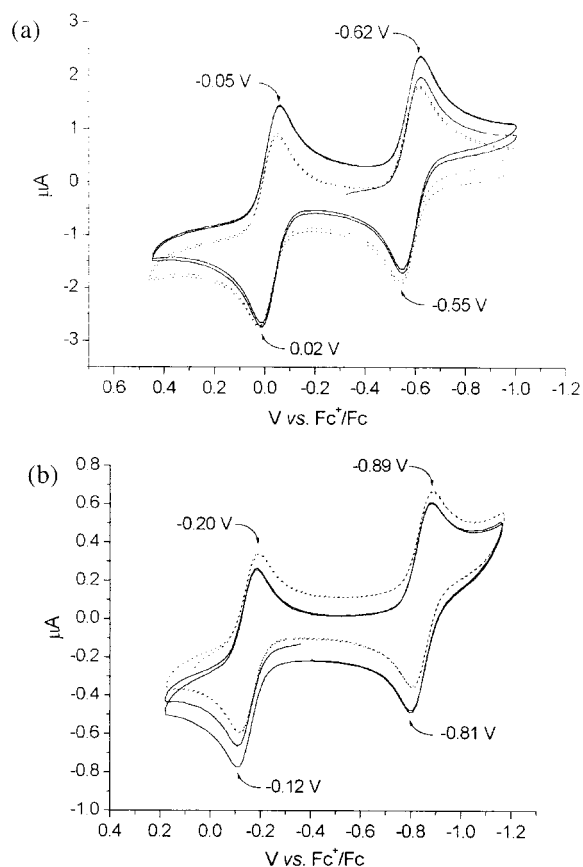

Figure 8. Cyclic voltammograms of (a) 1.0 mM DMF solution of 2·PPN$_2$ (···) and 3·PPN (−) and (b) 0.2 mM THF solution of 3·PPN (−) and 4 (····).
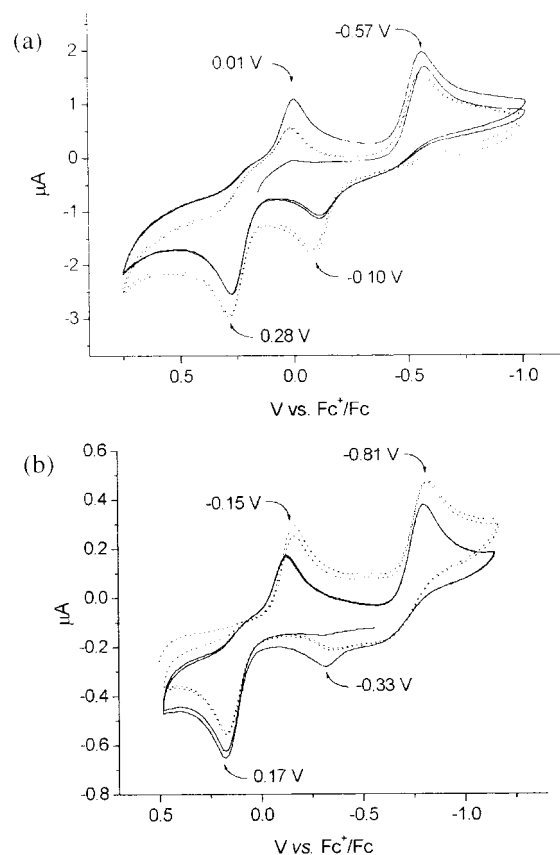

Figure 9. Cyclic voltammograms of (a) 1.0 mM DMF solution of 6·PPN$_2$ (···) and 7·PPN (−) and (b) 0.2 mM THF solution of 7·PPN (−) and 8 (···).

steric congestion between the carboranyl substituent and the thiolate proton.

Electrochemistry. Each redox step outlined in Schemes 1 and 2, except the step between 3 and 4, which involves the structural change in the cage C−C bond, can be conceptually considered as a combined outcome of the chemical redox of metal center, the intramolecular redox between the metal and the cage, and the cage structural change. Despite the complex feature of the step, it appears reversible on the bulk synthetic time scale. But, the electrochemical analysis indirectly reveals the complex nature associated with the foregoing steps.

For the two sets of three-component molybdenum and tungsten redox systems, each compound was used to obtain a cyclic voltammogram covering the entire potential range of interest, and two different solvent systems were employed for this end due to the solubility property. The cyclic voltammograms of 2·PPN$_2$ and 3·PPN in DMF and 3·PPN and 4 in THF (Figure 8) show typical reversible patterns. The comparison of the redox potentials in both cases supports that the molybdacarboranes are related to each other not only by chemical redox process, as shown in Scheme 1, but also by pure electronic redox process. On the other hand, the cyclic voltammograms of 6·PPN$_2$ and 7·PPN in DMF and 7·PPN and 8 in THF (Figure 9) show a different pattern: It appears irreversible from the redox couple point of view, but the reversible pattern of the overall cycle is distinct after multiple scans. The redox potentials of the complexes in both cyclic voltammograms imply that three tungstacarboranes constitute the same family of a redox cycle. The irreversibility of the cyclic voltammograms from the redox couple point of view support the presence of the complex reaction nature in the redox step involving the structural change in the cage C−C bond.

of "switch off/switch on" (in other words, electron-losing/electron-keeping for the metal point of view). It is interesting to note that even a small difference (0.1) in electronegativity of the metal center leads to a clear structural change in the cage.

Attempts to control the electron-withdrawing power of the carborane cage by introducing substituents to the carborane carbon atoms were not successful. When [(C$_2$B$_9$H$_9$R$_1$R$_2$)Mo-(CO)$_3$]·PPN$_2$ (R$_1$, R$_2$ = H, Me or Me, Me) and PhSSPh were reacted under refluxing temperature, only *nido*-C$_2$B$_9$H$_{10}$R$_1$R$_2$$^-$ was observed in the in situ B NMR study, which implies the total decomposition of the complexes, presumably due to the

Conclusion

A series of molybdenum and tungsten complexes $[(C_2B_9H_{11})M-(\mu\text{-SPh})_2]_2^n$ (M = Mo, W; $n = 2-, 1-, 0$), whose synthesis and structures are reported in this paper, constitutes the first examples involving the reversible C−C cleavage ↔ C−C formation process, or "switch off ↔ switch on" conversion, in the nonsubstituted 12-vertex systems. Cage distortion vs electron buffer feature of the dicarbollide ligand is clearly seen in this series. The "switch off" systems that are considered as the manifestation of the cage distortion feature of the dicarbollide ligand invoke the presence of a new kind of deformed cage, the semicloso framework driven by the intramolecular redox reaction. The "switch on" systems reflect the electron buffer ability of the dicarbollide ligand. The "switch off ↔ switch on" conversions are triggered by the external redox of the metal center and proceed via the intramolecular redox reaction followed by the cage structural change. In particular, the deformed cages seen in **2**·PPN₂, **6**·PPN₂, and **7**·PPN spurs the study of the competition of electrons between the metal and the carborane cage and thus opens a new field in the metallacarborane chemistry.

Supporting Information Available: Listings of the experimental crystallographic data, the positional and equivalent isotropic thermal parameters, the anisotropic thermal parameters, the bond distances and angles, and the XPS interpretations for **2**·PPN₂, **3**·PPN, **4**, **6**·PPN₂, **7**·PPN and **8**; ¹H−¹H COSY NMR spectra of **2**·PPN₂ and **6**·PPN₂ (PDF). This material is available free of charge via the Internet at http://pubs.acs.org.

JA0106265